Testing the basin-centered gas accumulation model using fluid inclusion observations: Southern Piceance Basin, Colorado

András Fall, Peter Eichhubl, Stephen P. Cumella, Robert J. Bodnar, Stephen E. Laubach, and Stephen P. Becker

ABSTRACT

The Upper Cretaceous Mesaverde Group in the Piceance Basin, Colorado, is considered a continuous basin-centered gas accumulation in which gas charge of the low-permeability sandstone occurs under high pore-fluid pressure in response to gas generation. High gas pressure favors formation of pervasive systems of opening-mode fractures. This view contrasts with that of other models of low-permeability gas reservoirs in which gas migrates by buoyant drive and accumulates in conventional traps, with fractures an incidental attribute of these reservoirs. We tested the aspects of the basin-centered gas accumulation model as it applies to the Piceance Basin by determining the timing of fracture growth and associated temperature, pressure, and fluid-composition conditions using microthermometry and Raman microspectrometry of fluid inclusions trapped in fracture cement that formed during fracture growth. Trapping temperatures of methane-saturated aqueous fluid inclusions record systematic temperature trends that increase from approximately 140 to 185°C and then decrease to approximately 158°C over time, which indicates fracture growth during maximum burial conditions. Calculated pore-fluid pressures for methane-rich aqueous inclusions of 55 to 110 MPa (7977–15,954 psi) indicate fracture growth under near-lithostatic pressure conditions consistent with fracture growth during active gas maturation and charge. Lack of systematic pore-fluid–pressure trends

Manuscript received October 5, 2011; provisional acceptance January 9, 2012; revised manuscript received March 2, 2012; final acceptance May 17, 2012.
DOI:10.1306/05171211149

AUTHORS

ANDRÁS FALL ~ *Bureau of Economic Geology, John A. and Katherine G. Jackson School of Geosciences, University of Texas at Austin, Austin, Texas; andras.fall@beg.utexas.edu*

András Fall is a research associate at the Bureau of Economic Geology. He received a B.S. degree in geology and geography from the Babe Bolyai University, Cluj-Napoca, Romania, and an M.S. degree and a Ph.D. in geosciences from Virginia Tech. His research interests involve the function and properties of fluids in geologic and geochemical processes using fluid inclusions, and interaction of fluids and natural fractures in diagenetic environments.

PETER EICHHUBL ~ *Bureau of Economic Geology, John A. and Katherine G. Jackson School of Geosciences, University of Texas at Austin, Austin, Texas; peter.eichhubl@beg.utexas.edu*

Peter Eichhubl is a research scientist at the Bureau of Economic Geology. He received an M.S. degree in geology from the University of Vienna, Austria, and a Ph.D. in geology from the University of California, Santa Barbara. His research combines fault and fracture mechanics and low-temperature geochemistry, deformation mechanisms of the upper crust, and structural control of mass and heat transfer in sedimentary basins. He supervises graduate students and postdoctoral scholars within the Jackson School of Geosciences.

STEPHEN P. CUMELLA ~ *Endeavour International Corporation, Denver, Colorado; steve.cumella@endeavourcorp.com*

Stephen P. Cumella is a geologist at Endeavor International Corporation in Denver, Colorado. He received his M.S. degree from the University of Texas at Austin. He is an expert in tight-gas sandstone reservoirs in the Piceance Basin and other Rocky Mountain basins.

ROBERT J. BODNAR ~ *Fluids Research Laboratory, Department of Geoscience, Virginia Tech, Blacksburg, Virginia; rjb@vt.edu*

Robert J. Bodnar is a university distinguished Professor and C. C. Garvin Professor of Geochemistry. He received a B.S. degree in

chemistry from the University of Pittsburgh, an M.S. degree in geology from the University of Arizona, and a Ph.D. in geochemistry and mineralogy from Penn State University. His research involves the distribution, properties, and function of fluids in Earth and planetary systems through experimental and theoretical studies of fluid inclusions and other geologic and geochemical processes. He supervises graduate students within the Department of Geosciences, Virginia Tech.

STEPHEN E. LAUBACH ~ *Bureau of Economic Geology, John A. and Katherine G. Jackson School of Geosciences, University of Texas at Austin, Austin, Texas; steve.laubach@beg.utexas.edu*

Stephen E. Laubach is a senior research scientist at the Bureau of Economic Geology. He received a B.S. degree in geology from Tufts University and an M.S. degree and a Ph.D. in geology from the University of Illinois at Urbana. He conducts research on fractured and unconventional reservoirs and structural diagenesis. He supervises graduate students within the Jackson School of Geosciences.

STEPHEN P. BECKER ~ *ExxonMobil Upstream Research Company, Houston, Texas; stephen.becker@exxonmobil.com*

Stephen P. Becker is a geochemist at ExxonMobil Upstream Research Company in Houston. He received B.S. and M.S. degrees in geology from the University of Missouri at Rolla and a Ph.D. in geochemistry from Virginia Tech. His research interests focus on the function of fluids in basinal environments and applications of fluid inclusions to reconstructing basin history and fluid properties in hydrocarbon exploration, development, and production.

ACKNOWLEDGEMENTS

We thank Michael Dempsey, Jeff Balmer, Tim Baer, and T. J. Dewane of EnCana Oil and Gas for discussions, core access, and permission for data release. We also thank John Hooker and Rob Reed for assisting with scanning electron microscopy–catholuminescence imaging, and Charles Farley, with Raman analyses. We thank former AAPG Editor Ernest A. Mancini for presiding over the editorial review of this paper.

over time suggests dynamic pressure conditions requiring an active process of pressure generation during maximum burial conditions. Such a process is consistent with gas generation within the Mesaverde Group or by gas charge from deeper source rocks along fracture and fault systems but is inconsistent with significant high-pressure generation by compaction disequilibrium during earlier stages of burial. On the basis of a comparison of trapping temperatures with burial and thermal maturity models, we infer that active gas charge and natural fracture growth lasted for 35 m.y. and ended at approximately 6 Ma. Our results demonstrate that protracted growth of a pervasive fracture system is the consequence of gas maturation and reservoir charge and is intrinsic to basin-centered gas reservoirs.

INTRODUCTION

Tight-gas sandstones are a significant unconventional resource for natural gas, but their charge mechanisms and the function of natural fractures during gas charge continue to be debated. Tight-gas sandstones of the Cretaceous Mesaverde Group in the Piceance Basin, Colorado (Figures 1, 2), have been considered continuous basin-centered gas accumulations (Brown et al., 1986; Johnson, 1989; Law, 2002; Schmoker, 2002; Law and Spencer, 2004; Cumella and Scheevel, 2008; Cumella, 2009). Such a system is characterized by gas-prone source rocks and low-permeability reservoirs in close proximity to one another, a lack of downdip water contacts, and gas accumulations that grade vertically across stratigraphic boundaries, forming a continuously saturated gas interval in the deeper parts of the basin (Figures 2; 3A; 4). In the Piceance Basin, the top of gas is marked by a transition from gas to mixed water and gas and into a gas-free water zone (Figures 3A; 4) (Law, 2002; Cumella and Scheevel, 2008). The primary trapping mechanism in these low-permeability (<0.1 md; 1 md = 10^{-3} d) rocks is capillary resistance, with generally high capillary entrance pressure at moderate saturation of the wetting phase (Law and Dickinson, 1985; Spencer, 1989a; Law, 2002; Law and Spencer, 2004). With continued burial and gas generation, the system becomes sufficiently overpressured to overcome the high capillary entrance pressure of the tight matrix and to expel water from the pores, resulting in an overpressured gas-saturated interval with little residual water. Pore pressures and pore-fluid–pressure gradients during gas charge are thus expected to be above hydrostatic.

The presence of natural fractures is an important component of the system, providing gas-migration pathways during

charge and connectivity between matrix pores, hydraulic fractures, and the wellbore during production (Laubach, 1988, 2003; Lorenz and Finley, 1991; Lorenz and Hill, 1994; Cumella and Scheevel, 2008; Cumella, 2010). High pore-fluid pressures during gas generation would favor fracture opening and growth (Olson et al., 2009). Fracture formation would thus be expected to be contemporaneous with gas generation and charge. Fracture opening and subsequent sealing by mineral precipitation can provide transient migration pathways and, therefore, dynamic pore-fluid–pressure conditions over time. Regions of higher-than-average permeability and production, or sweet spots, have been attributed to the presence of open natural fractures (Surdam, 1997; Laubach, 2003).

A different view was put forward by Shanley et al. (2004) and Camp (2008), describing some Rocky Mountain tight-gas reservoirs, such as those in the Greater Green River Basin, as low-permeability reservoirs in which gas accumulates in subtle conventional stratigraphic and structural traps (Figure 3B), and gas charge is driven primarily by buoyancy. These workers contended that low-permeability sandstones have unique petrophysical properties and that the failure to understand these properties has led to a misunderstanding of fluid distribution in the subsurface. In a conventional reservoir with good permeability, water-free gas is produced updip from an interval in which both gas and water are produced, which in turn overlies free-water production below a gas-water contact. In low-permeability sandstone reservoirs, gas production is generally restricted to sandstones with water saturations of less than 50%, and in sandstones with water saturations of greater than 50%, the relative permeability to either gas or water is so low that little to no fluid flow exists (Figure 3B). The term "permeability jail" was coined to describe this phenomenon. Shanley et al. (2004) proposed that this lack of fluid flow in sandstones with higher water saturations has led to the misperception that large areas in the deeper parts of Rocky Mountain basins are pervasively gas saturated.

Cumella (2010) suggested that hydrocarbon column heights in the discontinuous fluvial sandstone bodies of Piceance tight-gas reservoirs would be insufficient to attain sufficiently high reservoir pressures resulting from buoyancy alone for gas emplacement into the tight pore structure. For example, capillary-pressure measurements of Mesaverde gas sandstones in the Piceance and other Rocky Mountain basins indicate that gas columns of several hundred feet to more than 305 m (1000 ft) are required to reach water saturations of 40% or less, which are typical of productive sandstones (Byrnes et al., 2009). However, productive sands in the Piceance

We thank Robert C. Burruss, Thomas Taylor, and Scott Wilkins for their detailed reviews that significantly contributed to the improvement of the paper. This study was supported by grant DE-FG02-03ER15430 from the Chemical Sciences, Geosciences, and Biosciences Division, Office of Basic Energy Sciences, Office of Science, U.S. Department of Energy; the Jackson School of Geosciences at the University of Texas at Austin; The GDL Foundation; and by industry sponsors of the Fracture Research and Application Consortium. The publication was authorized by the director, Bureau of Economic Geology, University of Texas at Austin.
The AAPG Editor thanks the following reviewers for their work on this paper: Robert Burruss, Thomas Taylor, and Scott J. Wilkins.

EDITOR'S NOTE

This paper was reviewed and accepted by sub-editor Ernest A. Mancini.

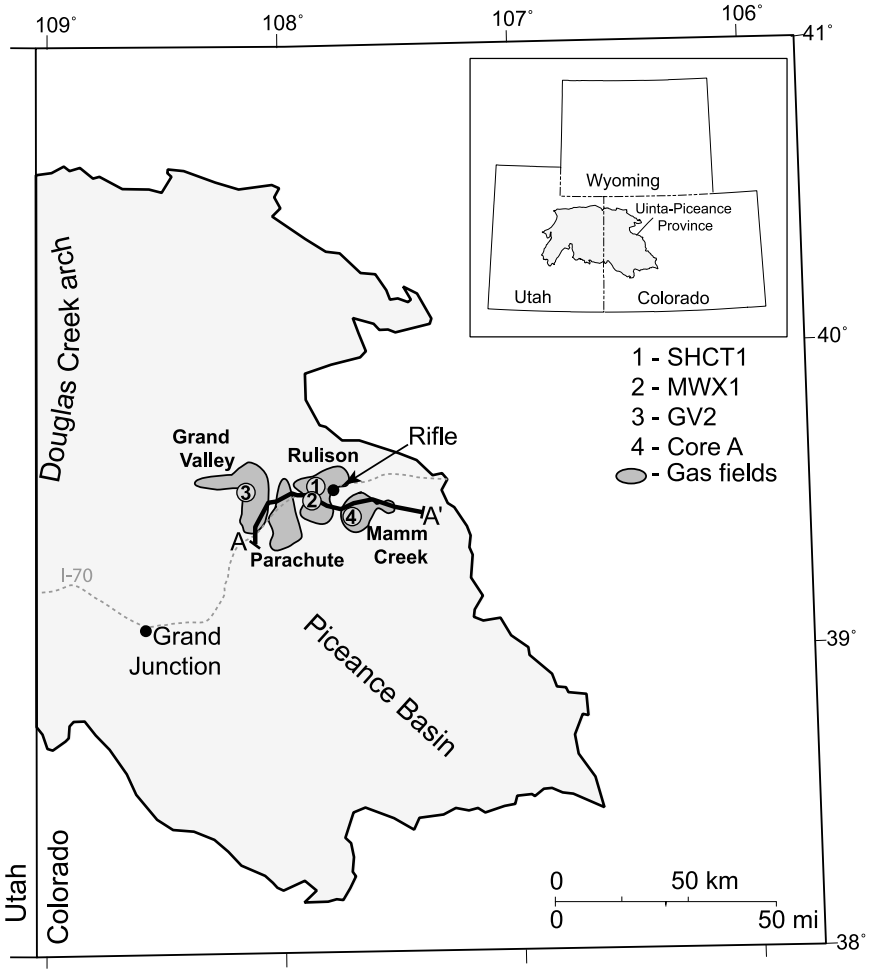

Figure 1. Well locations and gas fields in the southern Piceance Basin (modified from Nuccio and Roberts, 2003, and Cumella and Scheevel, 2008). Line AA' corresponds to the cross section in Figure 2.

Mesaverde accumulation average a few hundred feet in width and are typically more than 15 m (50 ft) thick (Lorenz et al., 1985), which is too small to allow buoyant force to charge sandstones with microdarcy permeability (Cumella, 2010). An alternative explanation for the creation of low water saturations is that the gas charge occurred before the sandstones reached very low permeability when the capillary forces required to reach low water saturations were much lower (Shanley et al., 2007). This explanation proposes that gas charge occurs at shallower burial depths and that compaction and cementation degrade permeability to the microdarcy range with continued burial (Figure 5).

This study was designed to test several aspects of the basin-centered gas accumulation model as it applies to the Piceance Basin. We selected aspects that we consider characteristic to the basin-centered gas accumulation model and that would not be expected if Piceance Basin tight-gas accumulations formed by buoyant drive in conventional traps. In addition, we selected aspects that can be tested with fluid inclusion techniques. These aspects include (1) the timing of gas charge and fracture opening relative to the burial and host-rock diagenetic history and (2) the magnitude and history of overpressure development in the reservoir during fracture opening. According to Law (2002), gas charge in basin-centered gas accumulations occurs near or at peak burial temperature and depth conditions. In contrast, following Shanley et al. (2004, 2007), gas charge occurs before peak burial, before porosity is occluded and permeability is reduced to microdarcy levels. High pore-fluid pressures are inherent to the basin-centered gas model, with high pressures limited by the fracture gradient. Pressure buildup is thus

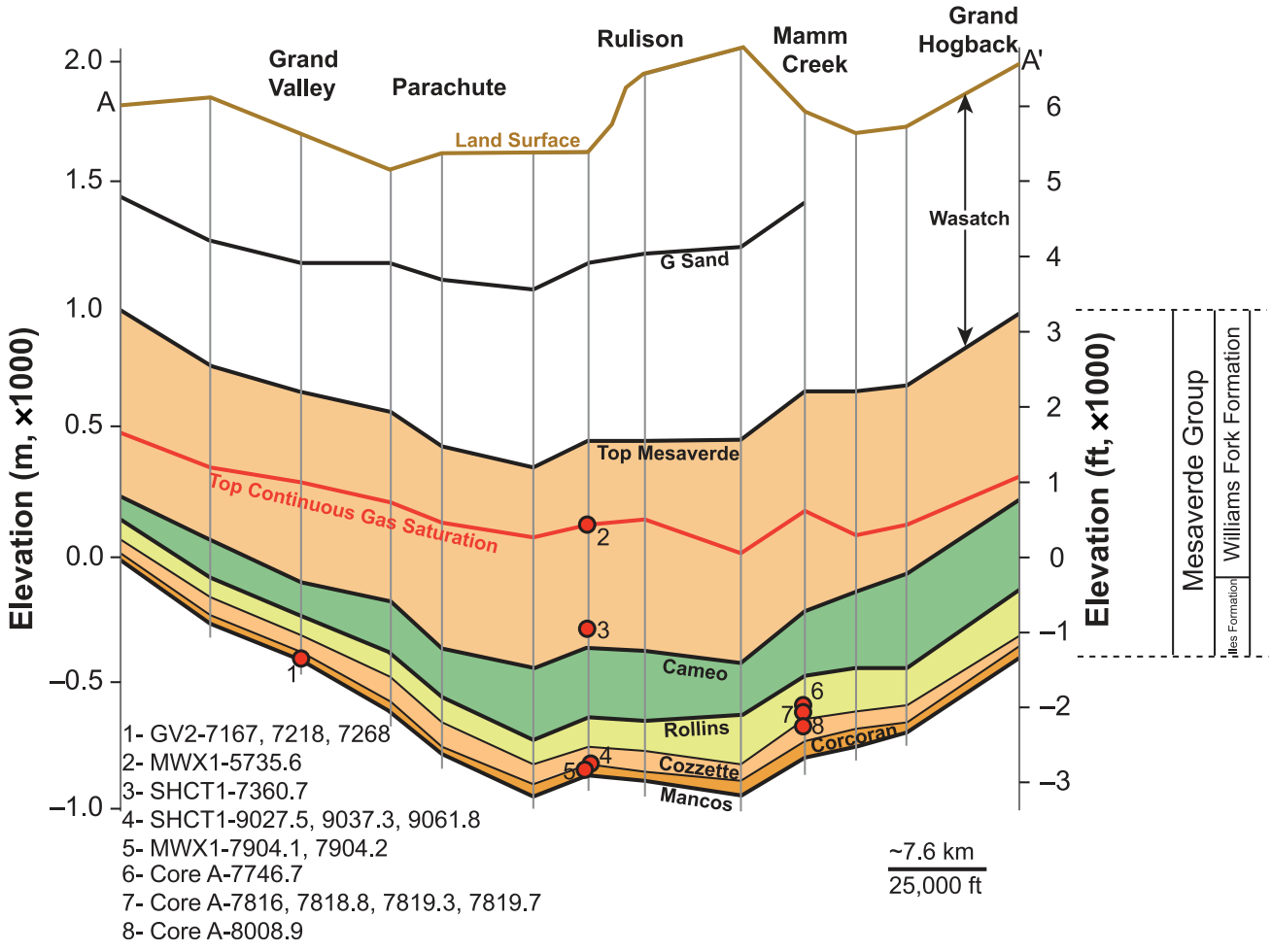

Figure 2. Structural cross section of the Mesaverde Group along line AA′ (Figure 1) (modified from Cumella and Scheevel, 2008). Red circles are depths of sample locations.

expected to be coeval with natural fracture opening. A mechanism for high abnormal pore-fluid pressure and related formation of fractures, or for dynamically varying pore-pressure conditions, is not inherent in the Shanley et al. (2004) model but likely to occur before peak burial during gas migration into conventional traps. We tested these hypotheses by fluid inclusion analyses of natural quartz-cemented fractures sampled in core along an east-west transect across the southern Piceance Basin. Fluid inclusions contained in fracture-filling cement that precipitated during fracture opening were analyzed by microthermometry and Raman microspectrometry to obtain a history of temperature, pore-fluid pressure, and fluid composition. The relative timing of the fluid inclusion assemblages (FIAs) is constrained by textural mapping of fracture-growth cement zones. This record is then compared with burial history and thermal maturity models so as to relate fracture formation and pore-fluid–pressure evolution to burial depth and gas production and charge.

We show that the formation of open fractures is concurrent with gas generation close to the maximum burial depth and under near-lithostatic pore-fluid pressures. Reservoir charge and fractures coevolved, and open fractures are pervasive attributes of this gas accumulation. This process is consistent with fracture formation, gas charge, and diagenetic porosity loss as persistent and pervasive characteristics of these reservoirs. Our model does not preclude the occurrence of conventional traps, but our findings are consistent with gas-charge processes commonly associated with basin-centered gas accumulations.

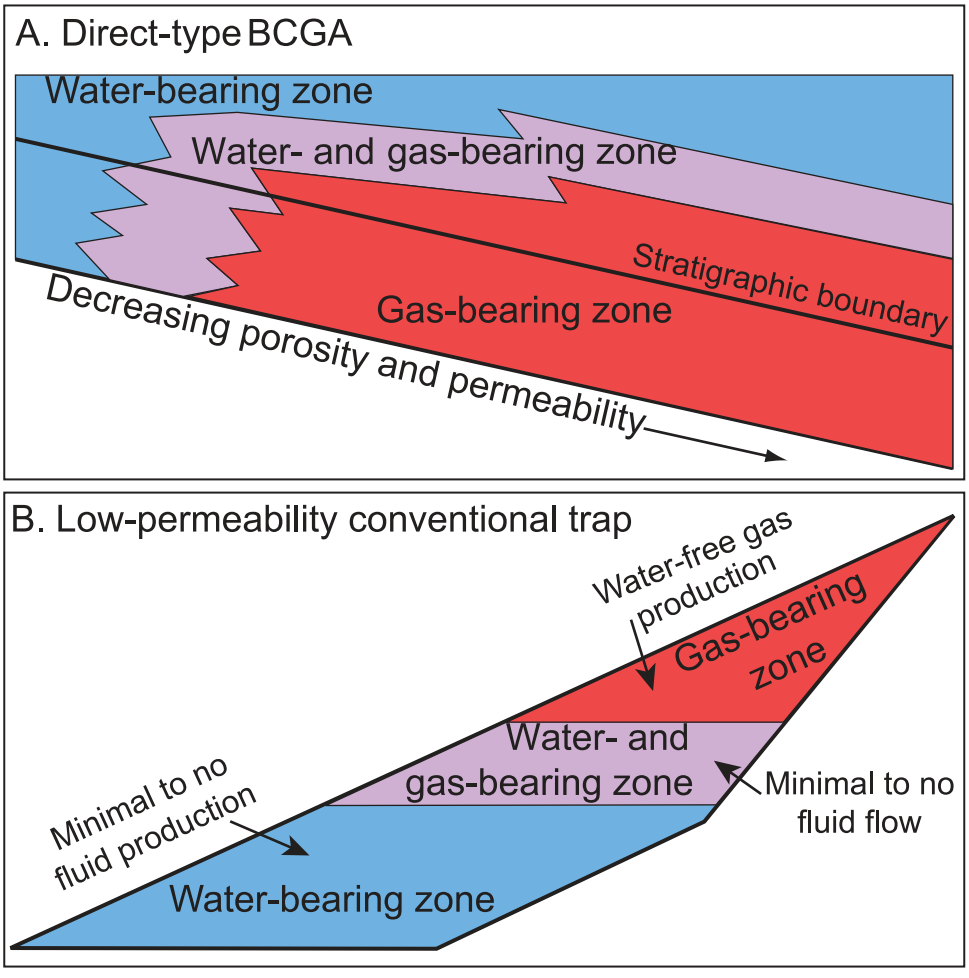

Figure 3. Simplified models of tight-gas sandstone reservoirs. (A) Direct-type basin-centered gas accumulation (BCGA) (modified from Law, 2002; used with permission of AAPG). (B) Low-porosity conventional trap (modified from Shanley et al., 2004; used with permission of AAPG).

GEOLOGIC SETTING

The Piceance Basin is an elongate, northwest-southeast–trending, asymmetric intermontane basin in northwestern Colorado (Figure 1), formed during the Late Cretaceous and the Paleogene (Johnson and Nuccio, 1986; Johnson and Rice, 1990; Cumella and Ostby, 2003; Patterson et al., 2003; Zhang et al., 2008; Cumella, 2009). The approximately 1400-m (~4600-ft)–thick Upper Cretaceous Mesaverde Group is composed of the Iles and Williams Fork formations (Figure 2). In the southern Piceance Basin, the Iles Formation overlies the marine Mancos Shale and includes three laterally continuous marine sandstones, the Corcoran, Cozzette, and Rollins members, which are separated by tongues of Mancos Shale (Figure 2). The Williams Fork Formation is a sequence of nonmarine shales, discontinuous sandstones, and coals that were deposited on a coastal plain (Cumella and Ostby, 2003; Nelson, 2003b; Cumella and Scheevel, 2008).

The low-permeability sandstones in the Mesaverde Group contain subvertical natural fractures (Verbeek and Grout, 1984a, b; Pitman and Sprunt, 1987; Lorenz and Finley, 1991; Lorenz and Hill, 1994; Cumella and Scheevel, 2008; Hooker et al., 2009). Sampling with vertical and direction cores shows that fractures are widespread (Lorenz and Hill, 1994; Hooker et al., 2009). The predominant strike of the fractures is west-northwest–east-southeast, but locally, the strike changes to east-west in the western part of the basin (Pitman and Sprunt, 1987; Lorenz and Finley, 1991; Cumella and Ostby, 2003; Cumella and Scheevel, 2008). The fractures we described are mostly open, despite local quartz-cement bridges that contain fluid inclusions. In this, the

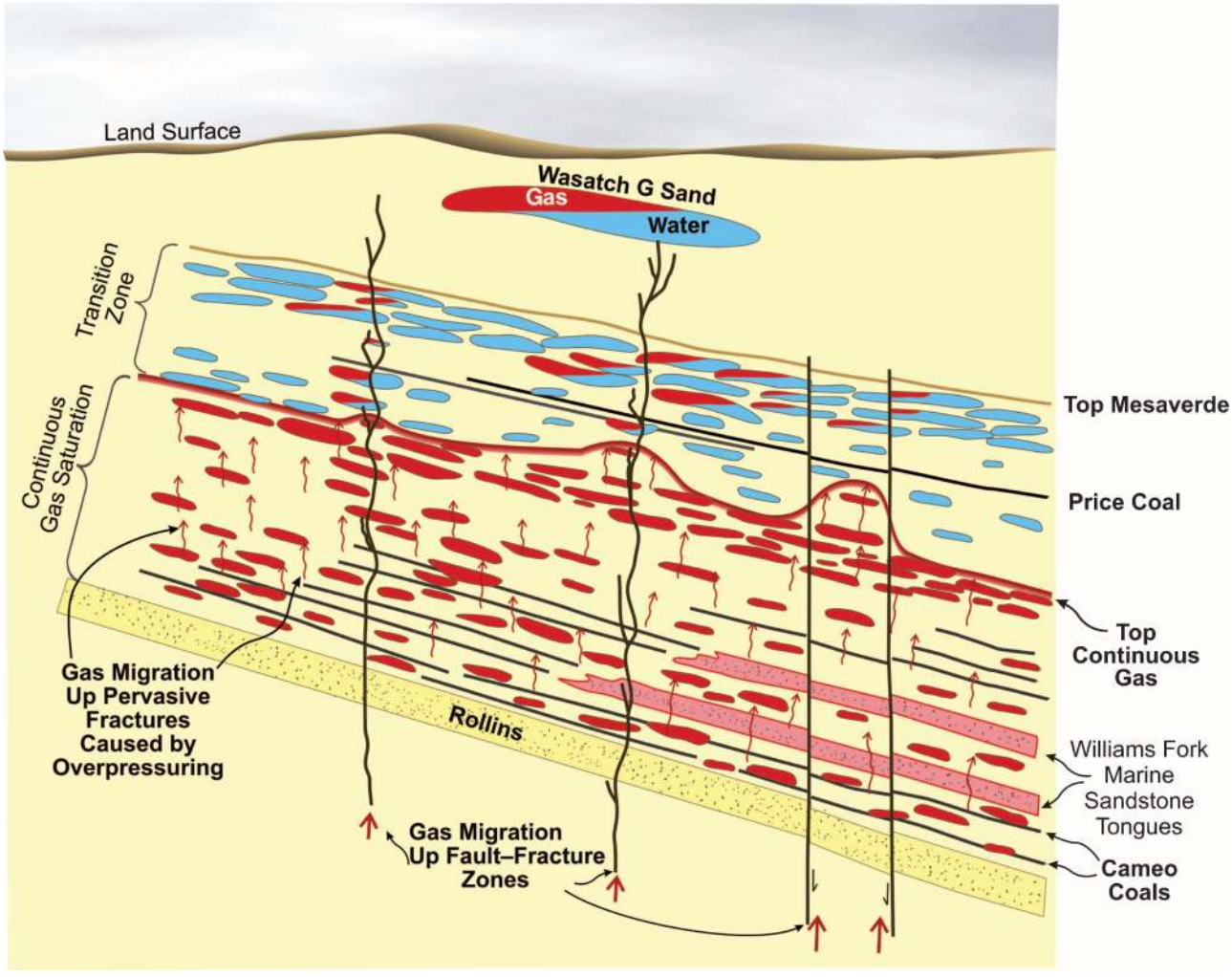

Figure 4. Cross section illustrating a gas-migration model for the Mesaverde Group in the southern Piceance Basin, Colorado (modified from Cumella and Scheevel, 2008; used with permission of AAPG). Coals and shales in and below the Mesaverde generate gas that overpressures the reservoirs, creating a pervasive natural fracture network (small arrows) that allow upward gas migration and formation of a continuous gas-saturated interval. Ovoid shapes represent fluvial sandstone bodies that are pervasively charged below the top of continuous gas (red color) or are wet (blue color) or partially charged (blue and red colors) above the top of continuous gas saturation. Williams Fork marine sandstone tongues (pink color) are also gas saturated. Migration of highly pressured gas from the underlying Mancos Shale also likely occurs along major faults. Sandstones adjacent to these fault zones are predicted to be highly gas charged, whereas sandstones in areas of poorly connected fracture systems are inferred to receive lesser gas charge with higher resultant water saturations.

fractures resemble those in many other tight-gas sandstones (Laubach et al., 2004a). Locally, quartz-lined fractures are filled with calcite that was mostly deposed after fractures ceased opening, again, in a pattern similar to that of many tight-gas sandstones (Laubach, 2003). Fractures are limited mostly to sandstone reservoirs without crossing into adjacent shale layers because of the differences in mechanical properties of the sandstone and shale layers.

Several different data sets provide evidence of a pervasive fracture system in the Mesaverde sandstones. The great disparity between sandstone-matrix permeabilities (microdarcys) and reservoir permeabilities measured by long-term pressure tests of individual Williams Fork sandstone reservoirs (tens to hundreds of microdarcys) is best explained by the presence of abundant natural fractures (Lorenz et al., 1989). Furthermore, diagnostic fracture injection–falloff test data from

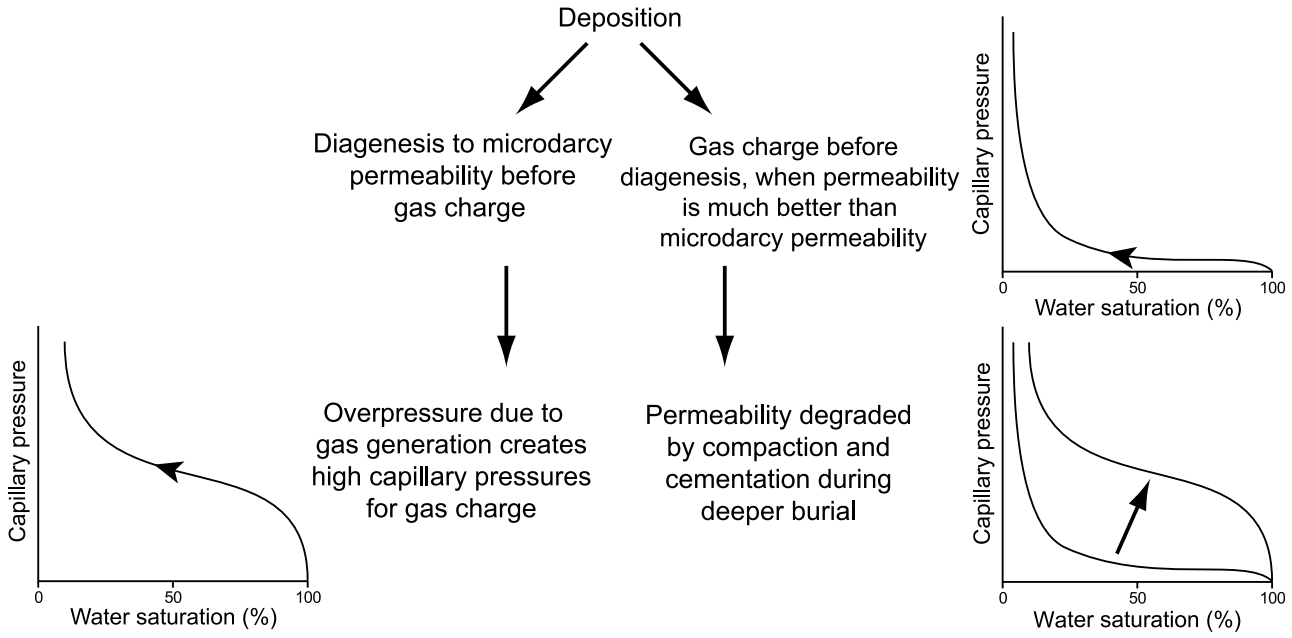

Figure 5. Different pathways for microdarcy sandstones to reach current water saturations of less than 50%.

810 tests showed that 61% of the tests had pressure-dependent leakoff, indicating the presence of natural fractures (Craig et al., 2005). Additional evidence of abundant natural fractures is provided by numerous image logs that have been obtained in the Piceance Basin in recent years (Koepsell et al., 2003).

An extensive test combining wireline logging, borehole seismic, and surface seismic data was recently conducted in the northern Piceance Basin for seismic characterization of natural fractures (Lewallen et al., 2008). In this study, dipole sonic logs showed that little to no shear-wave anisotropy is measured from the surface to the top of the gas-saturated interval. Within the gas-saturated interval, anisotropy in the sandstones is pronounced, ranging from 5 to 20%, whereas anisotropy in the shales never exceeds 5%. The authors propose that shear-wave anisotropy is controlled primarily by the presence of natural fractures because shear waves travel faster parallel to natural fractures than perpendicular to them. The pronounced anisotropy within the gas-saturated interval and the lack of anisotropy above it support the model that extensive natural fracturing is associated with gas generation. The correlation between the orientation of fast shear-wave azimuth from the dipole sonic log and the orientation of the natural fractures in the image logs is excellent.

Throughout the Mesaverde Group, natural fractures in core show dominant opening-mode displacement, with a wide range of aperture sizes of as much as 1.0 cm (0.4 in.) at all depths (Hooker et al., 2009; Hooker and Laubach, 2010) and varying degrees of mineralization. Quartz is commonly present as fracture cement, although it is not always obvious in hand samples. Calcite and clay minerals are locally prominent (Lorenz and Finley, 1991). For our study, core samples containing quartz cement were collected from the deeper parts of the Mesaverde Group in the Grand Valley (Barrett Energy Company Grand Valley 2 Federal, from now on GV2), Rulison (U.S. Department of Energy and CER Corporation core MWX1, from now on MWX1; and U.S. Department of Energy and CER Corporation core SHCT1, from now on SHCT1), and Mamm Creek (EnCana Core A, original well name changed because of confidentiality) areas (~1.09–1.52-mi [1.75–2.45-km], ~1676–2438-m [5500–8000-ft] depth interval), corresponding to the lower parts of the Williams Fork and Iles formations (Figures 1, 2; Table 1).

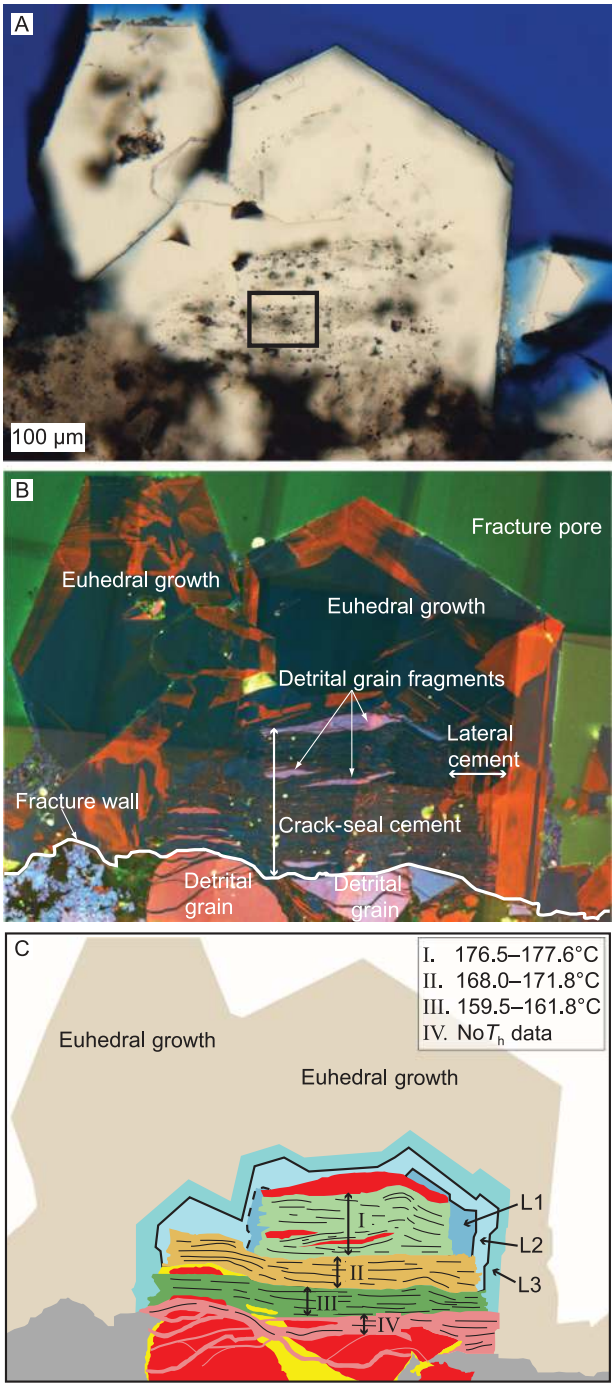

Figure 6. Photomicrograph and cathodoluminescence images of quartz cement in a partly cemented fracture (sample SHCT1-7360.7_1). (A) Transmitted light; the rectangle corresponds to Figure 7. (B) Scanning electron microscopy–cathodoluminescence image. (C) Textural reconstruction of crack-seal cement stages 1 to 4 and lateral cement stages L1 to L3. Apparent onlap of lateral cements L2 and L3 over stage 1 crack-seal cements is likely caused by the sample being cut at an angle to the *c* crystallographic axis of the euhedral overgrowth cement. T_h = homogenization temperature.

FRACTURE CEMENT PETROGRAPHY

Fractures partly cemented with quartz were impregnated with blue epoxy and prepared as doubly polished 50- to 60-µm–thick sections. Transmitted-light microscopy and scanning electron microscopy–cathodoluminescence (SEM-CL) imaging were used to examine fracture cement textures. Cathodoluminescence images were obtained using a Phillips XL30 SEM equipped with an Oxford Instruments MonoCL cathodoluminescence system, operated at 12 to 15 kV and large sample currents for CL images. Colored CL images were obtained by stacking three grayscale images collected using red, blue, and green filters. Images were adjusted for optimal color balance, contrast, and saturation during digital image processing.

Fractures contain quartz-cement bridges, euhedral quartz cement, and, locally, calcite cement. Quartz-cement bridges are defined as isolated cement occurrences that connect across fracture walls and that typically grow with the *c* crystallographic axis oriented roughly perpendicular to the fracture walls (Laubach, 1988; Laubach et al., 2004a; Becker et al., 2010). Quartz-cement bridges are commonly surrounded by fracture porosity or later cement. Similar to quartz-cement bridges described elsewhere (Laubach, 1988, 2003; Laubach et al., 2004b; Becker et al., 2010), quartz bridges contain an inclusion-rich core surrounded by inclusion-poor lateral cement (Figure 6A). The bridge core is composed of subparallel trails of fluid and solid inclusions oriented parallel to the fracture walls. We consider these fluid inclusion trails assemblages of cogenetic inclusions (FIAs) (Goldstein and Reynolds, 1994). Similar fluid inclusion trails are also observed in some quartz fracture cement that does not bridge both fracture walls but, instead, terminates into euhedral quartz (rectangle on Figures 6A; 7).

High-resolution SEM-CL imaging reveals that the inclusion-rich core of quartz-cement bridges is composed of multiple subparallel, 1- to 20-µm–wide quartz bands. Stacked transmitted-light and SEM-CL images of cement bridges reveal that the fluid inclusions are in the center of the crack-seal cement bands and that each cement band trapped

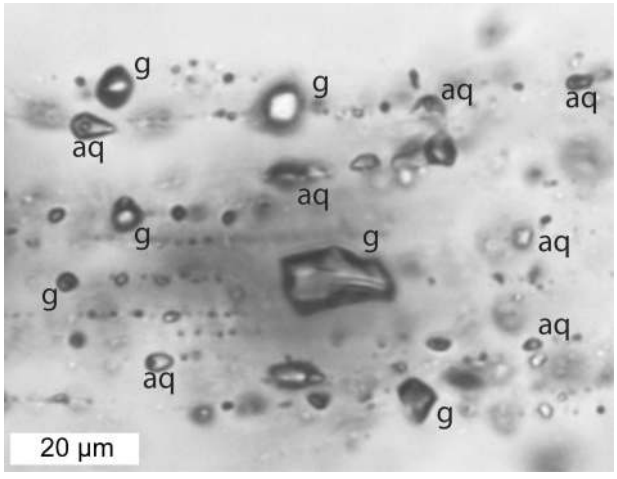

Figure 7. Photomicrograph of coexisting two-phase aqueous (aq) and single-phase gas (g) fluid inclusions in quartz cement shown in Figure 6A. Coexistence of gas-rich and aqueous fluid inclusions demonstrates trapping under gas-saturated conditions.

an individual FIA. Some of the cement bands crosscut previous bands marking sequential growth of cement bands. Fragments of detrital grains contained in bands are parts of broken and detached detrital grains observable on the fracture walls (Figure 6B). The multiple parallel cement bands, their mutual crosscutting relations, and the presence of detrital grain fragments among cement bands indicate repeated cycles of fracture opening and quartz precipitation, producing crack-seal texture (Ramsay, 1980; Laubach et al., 2004b). This crack-seal texture indicates that quartz-cement bridges formed concurrently (or synkinematically) with fracture opening. Inclusion-poor lateral cement of quartz bridges lacks crack-seal layers (Figure 6B) but contains idiomorphic growth layers, suggesting that lateral cement grew into open fracture space using the previously formed crack-seal bridge cement as a substrate.

Textural maps of crack-seal cement layers, lateral cements, and their mutual crosscutting relations (Figure 6C) allow interpretation of fracture opening and relative cement sequences (Laubach et al., 2004a; Becker et al., 2010). For example, quartz cement in sample SHCT1-7360.7_1 (Figure 6) initially grew synkinematically across the fracture by crack-seal mechanism (stage 1 in Figure 6C). With continued growth of crack-seal cement (stage 2 in Figure 6C), lateral idiomorphic cement (L1 in Figure 6C) deposited on the early crack-seal cement layers of stage 1, thus widening the bridge. Succeeding crack-seal increments of stages 2 to 4 cut across the increasingly wider cement bridge because of deposition of lateral cements L2 and, later, L3, resulting in longer crack-seal increments over time (Figure 6C). Subsequent to stage 4, the bridge pictured in Figure 6 detached from the opposing fracture wall, crack-seal cementation ceased, and quartz cementation continued as euhedral fracture cement. We interpret these cement occurrences as bridge fragments or failed bridges.

Stacked transmitted light and SEM-CL images reveal that the lengths of FIAs parallel to fracture walls correspond to the lengths of crack-seal cements. Thus, FIAs of crack-seal fracture cement record pressure, temperature, and fluid compositional conditions during fracture opening and a time segment of basin evolution.

FLUID INCLUSION ANALYSIS

At room temperature, FIAs trapped in crack-seal quartz cement contain coexisting two-phase, liquid-rich aqueous inclusions and single-phase liquid inclusions (Figure 7). The two-phase liquid-rich inclusions contain 5 to 10 vol. % vapor and range from less than 1 to 10 µm in size. The single-phase inclusions are less than 1 to 20 µm in size. Several FIAs containing large (10–30 µm) two-phase liquid-vapor inclusions are aligned perpendicular to the crack-seal layers. Based on stacked transmitted-light and SEM-CL images, we tentatively interpret these inclusions to postdate crack-seal cement growth and have not considered them further in interpreting the evolution of fracture opening and cementation.

Fluid inclusion microthermometry was performed before SEM-CL imaging to avoid possible beam damage to fluid inclusions. Microthermometric analyses of fluid inclusions were conducted using a Fluid, Inc.–adapted, U.S. Geological Survey–type, gas-flow heating-freezing stage mounted on an Olympus BX51 microscope equipped with a 40× objective (numerical aperture [NA] = 0.55) and 15× oculars. The stage was calibrated using the

Table 1. True Vertical Depth of Samples, and Type, Homogenization (Trapping) Temperatures, and Trapping Pressures of Fluid Inclusions in Quartz Fracture Cements in the Southern Piceance Basin, Colorado*

Sample Number	TVD** (ft)	G**	Aq** + G**	*T*** (°C)	*T*** (°F)	*P*** (MPa)	*P*** (psi, ×1000)
Grand Valley							
GV2-7167.0	7167.0		•	151–172	304–342	57–78	8.3–11.3
GV2-7218.0	7218.0	•					
GV2-7268.0	7268.0		•	154–163	309–325	55–68	8.0–9.7
Rulison							
MWX1-5735.6	5735.6	•					
SHCT-7360.7	~6900.0		•	140–178	284–352	61–98	8.8–14.2
MWX1-7904.1	7904.1		•	144–162	291–324	66–86	9.6–12.5
MWX1-7904.2	7904.2		•				
SHCT-9027.5	~7910.0	•					
SHCT-9037.3	~7910.0	•					
SHCT-9061.8	~7910.0		•	164–181	295–356	64–110	9.3–16.0
Mamm Creek							
Core A-7746.7	7746.7		•	157–168	315–334	75–93	10.9–13.5
Core A-7816.0	7816.0		•	157–161	315–322	83–88	12.0–12.8
Core A-7818.8	7818.8	•					
Core A-7819.3	7819.3	•					
Core A-7819.7	7819.7	•					
Core A-8008.9	8008.9	•					

*Bullet points indicate the presence of the respective fluid inclusion type.
**TVD = true vertical depth; G = gas; Aq = aqueous; *T* = temperature; *P* = pressure.

CO_2-ice–melting temperature at –56.6°C of H_2O-CO_2 synthetic fluid inclusions, the ice-melting temperature at 0°C, and the critical homogenization temperature at 374.1°C of pure H_2O synthetic fluid inclusion standards (Sterner and Bodnar, 1984). Liquid-vapor homogenization temperatures (T_h) were determined to ±0.05°C by thermal cycling using temperature steps of 0.1°C (Goldstein and Reynolds, 1994). Several individual fluid inclusions were measured in each FIA to assure the reliability of observed homogenization temperatures from each crack-seal cement layer. The T_h variation within individual FIAs was generally less than 3°C, suggesting that the inclusions were not reequilibrated after trapping (Bodnar, 2003). Homogenization temperature variations as a function of fluid inclusion size were not observed, probably as a result of the dissolved gas content of inclusions, which lowers the surface tension of the liquid-vapor interface (Fall et al., 2009). Final ice-melting temperatures were determined to ±0.1°C by the same thermal cyclic technique used in heating measurements.

Measured homogenization temperatures range from approximately 140 to 181°C throughout the sampled wells (Table 1; Figure 8). Several samples show clear trends in T_h from oldest to youngest crack-seal cement, as determined by SEM-CL textural mapping. These trends in T_h are interpreted to represent variations in fluid temperature during fracture opening and cementation, if T_h variations among inclusions within individual FIAs are significantly less than the overall T_h range for the sample. For example, the range in T_h for crack-seal fluid inclusions in sample SHCT1-7360.7_1 is 159.5 to 177.6°C (Figure 6), with T_h variation within a single FIA at 2 to 3°C. When T_h data are correlated with crack-seal cement stages on the interpreted CL image (Figure 6), we observe a decreasing temperature trend of 176.5 to 177.6°C for stage 1 cement, to 168.0 to 171.8°C in stage 2 cement, and to 159.5° to 161.8°C in stage 3 cement.

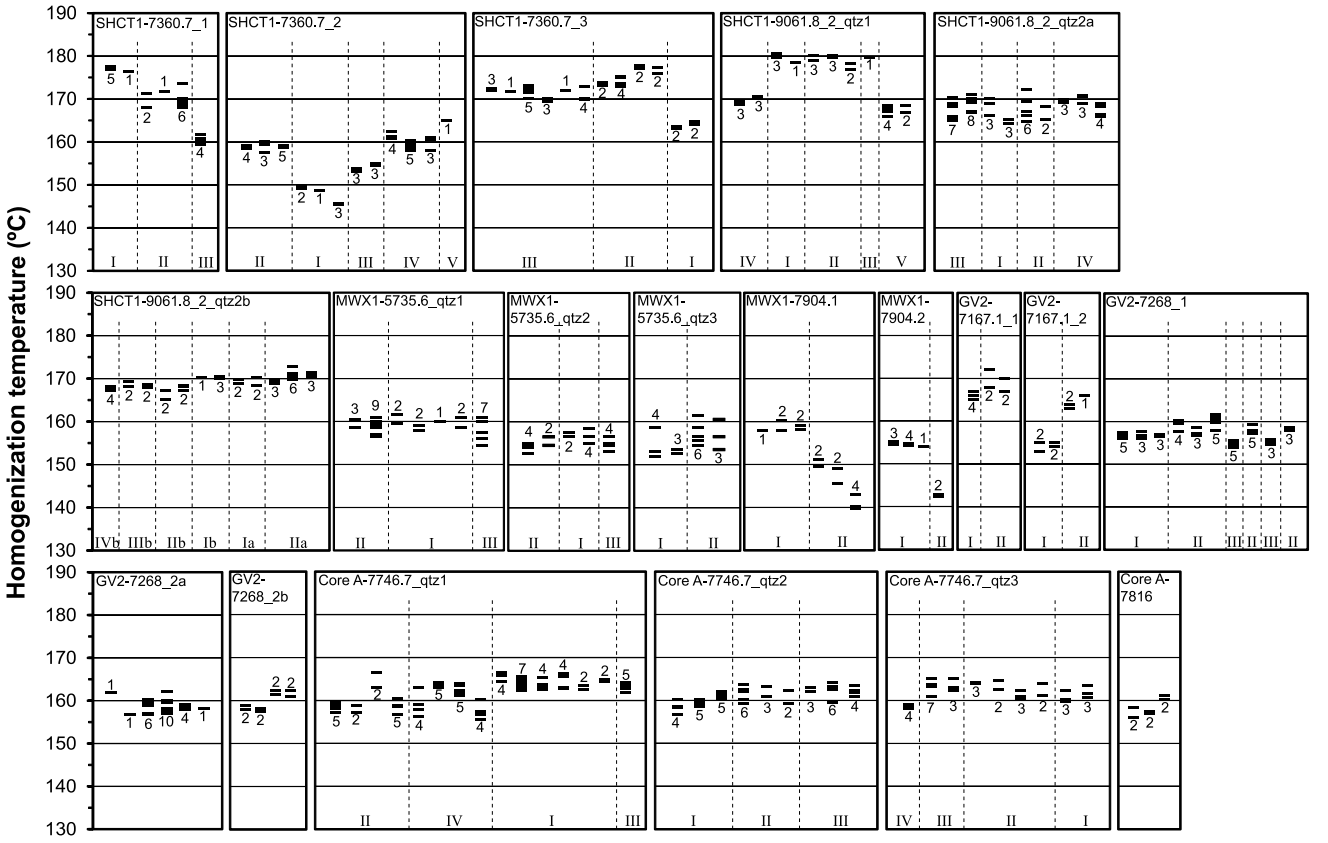

Figure 8. Homogenization-temperature (T_h) ranges for fluid inclusion assemblages (FIAs) in individual quartz bridges. The numbers in the diagrams represent the number of fluid inclusions within each FIA. Roman numerals indicate the relative timing of fracture opening and cementation stages based on textural interpretation of scanning electron microscopy–cathodoluminescence images. The FIAs on the diagrams mirror from left to right their respective position within the quartz bridges.

Whereas this failed bridge implies a partial opening history based on the fluid inclusion temperatures, many other cement bridges that entirely span the fractures show similar ranges and trends in decreasing or increasing homogenization temperatures, summarized in Figure 9. Several samples show minor or no temperature variation trends over time. Final ice-melting temperatures were recorded in the range of approximately –0.5 to –1.5°C, corresponding to salinities of 1.0 to 2.5 wt. % NaCl equivalent (Bodnar, 1993), with a dominant range at approximately 2 wt. % NaCl. Salinities are consistent throughout the samples and show no systematic trends with T_h during fracture cement growth. Eutectic ice-melting temperatures were not measured because of the small size of the inclusions.

Inclusions that are single phase at room temperature nucleate a vapor bubble during cooling and homogenize to the liquid phase within a range of –75 to –65°C, demonstrating that these single-phase inclusions contain a methane-dominated hydrocarbon fluid with a density above the critical density of the fluid mix (Goldstein and Reynolds, 1994). The presence of methane, ethane, and carbon dioxide in single-phase liquid inclusions was confirmed by Raman spectroscopy. These methane-rich and, at room temperature, single-phase inclusions were consistently observed alongside aqueous two-phase inclusions in all crack-seal cement samples, indicating that the pore fluid was saturated with methane and that a methane-rich hydrocarbon phase existed as a separate immiscible fluid phase at the time the fractures formed. The presence of methane in the aqueous inclusions was also confirmed using Raman spectroscopy. However, no ethane and/or carbon dioxide was detected in the

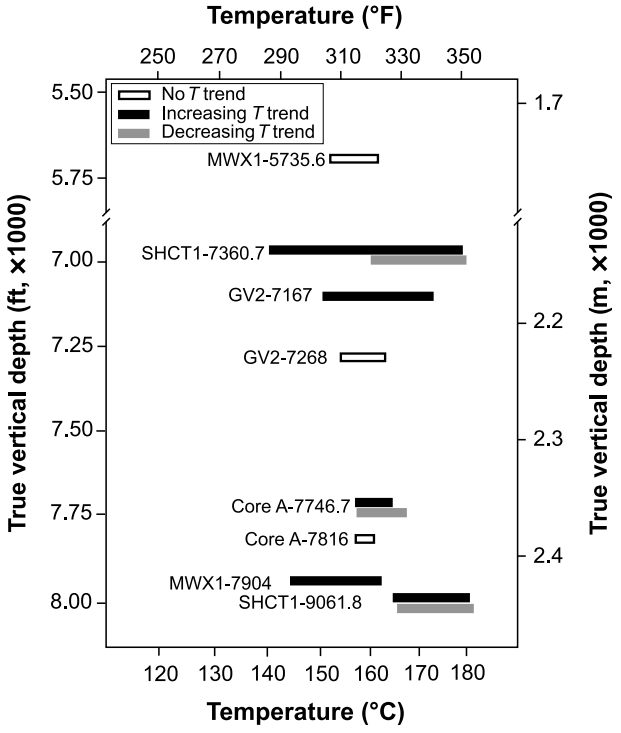

Figure 9. Ranges in fluid inclusion trapping (homogenization) temperatures (*T*) against the true vertical depth of fracture samples, southern Piceance Basin, Colorado.

aqueous inclusions. Coexistence of two-phase aqueous and single-phase hydrocarbon inclusions also indicates that fluid inclusions were trapped in the two-phase immiscible field. Measured homogenization temperatures thus represent trapping temperatures (Roedder, 1984; Goldstein and Reynolds, 1994).

Whereas single-phase methane-rich inclusions are consistently found in all the samples that we analyzed, aqueous two-phase inclusions are absent in several samples (Table 1). This absence of aqueous inclusions may reflect variations in gas saturation in the reservoir or, alternatively, in fluid-mineral wetting properties, resulting in preferential trapping of methane-rich fluid in some samples.

Trapping pressures were calculated following the procedures described by Becker et al. (2010) on the basis of Raman spectroscopic analyses of CH_4 within aqueous fluid inclusions (Lin et al., 2007). Raman analyses were conducted at Virginia Tech using a JY Horiba LabRAM HR (800-mm) spectrometer. The Raman spectra were collected with a laser beam being pointed at the vapor bubble in the aqueous fluid inclusions to determine the CH_4 Raman symmetric stretching (v_1) peak position. This peak position was used to determine the pressure in the inclusions at room temperature (Lin et al., 2007). However, we were not able to determine pressure for all inclusions with determined homogenization temperature (Figures 8, 9), because the motion of the vapor bubble in some of the inclusions precluded accurate analysis. Trapping pressures of fluid inclusions, where possible, were calculated on the basis of vapor-bubble pressure at room temperature, homogenization temperature, salinity of the aqueous fluid, and equations of state of Duan and Mao (2006). These calculations assume that the fluid is adequately characterized by the H_2O-NaCl-CH_4 system and the vapor phase by pure CH_4 (Becker et al., 2010).

Trapping pressures range from approximately 55 to 110 MPa (7977–15,954 psi) (Table 1) and are plotted in Figure 10A against estimated paleodepth. Also shown in Figure 10A are the hydrostatic gradient of 9.9 MPa/km (0.43 psi/ft) and the lithostatic gradient of 24.8 MPa/km (1.1 psi/ft) for comparison. The lithostatic gradient was calculated with a density of 2.53 g/cm^3, an estimate based on density-log data for the southern Piceance Basin. The hydrostatic gradient was calculated for a water column with an average seawater density of 1.02 g/cm^3. Whereas most calculated trapping pressures plot at moderately high to near-lithostatic pressures, two values plot above the lithostatic gradient. Becker et al. (2010) estimated that calculated fluid pressures using the technique used here are within 15% of the actual pressures. The above-lithostatic values are thus within the margin of error of these pressure estimates. Alternatively, or in addition, paleodepth estimation, which is based on a basin model (Nuccio and Roberts, 2003) and a calculated thermobaric gradient, could be inaccurate because of the small variation in density estimations, leading to variations in the lithostatic gradient.

Whereas homogenization (trapping) temperatures show consistent heating or cooling trends in many crack-seal cement samples (Figure 9), we find no consistent trends over time toward lower or higher trapping pressures. Instead, trapping pressures among different FIAs in the same cement

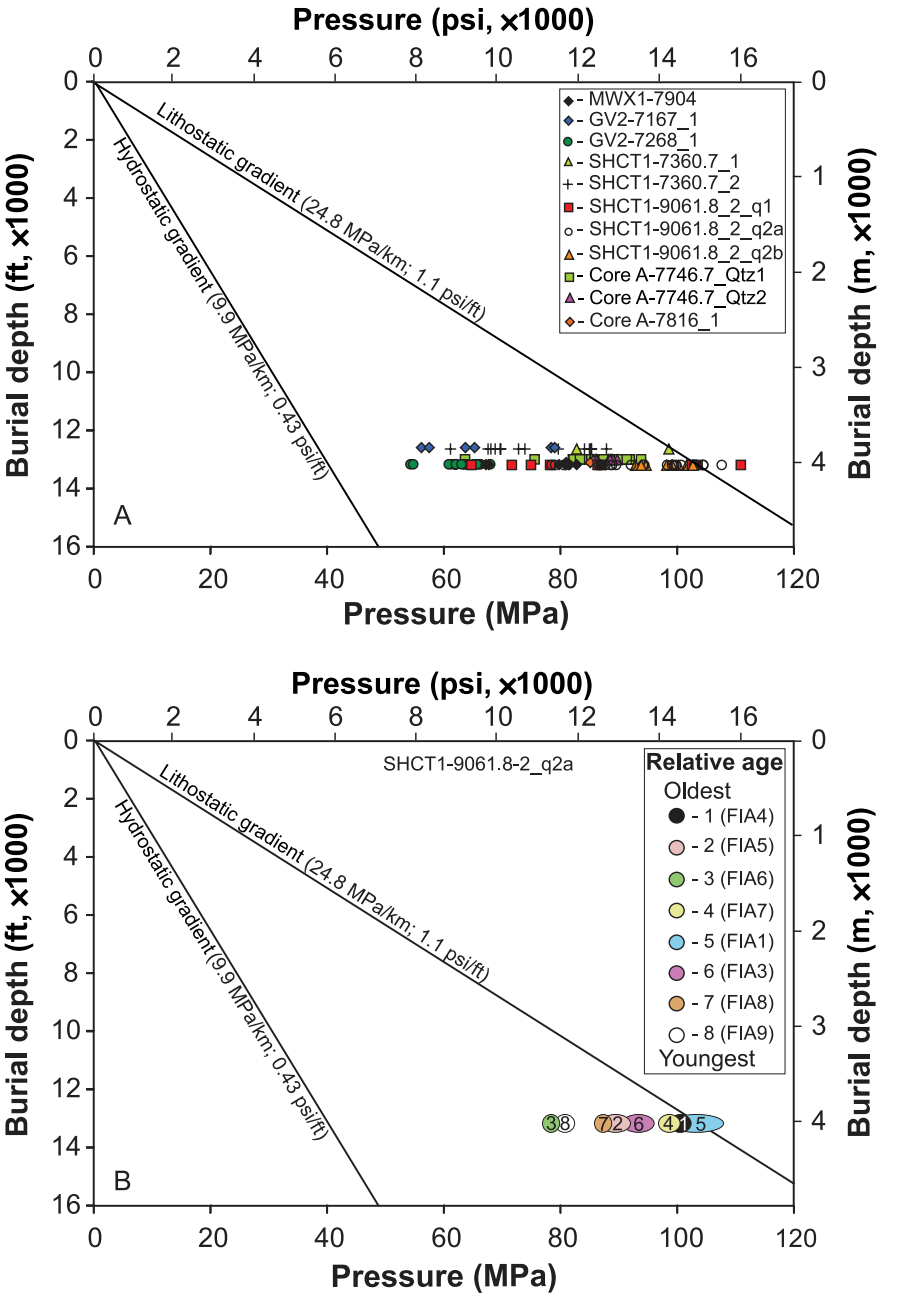

Figure 10. (A) Calculated fluid inclusion trapping pressure against inferred maximum burial depth. (B) Sequence of trapping pressures for sample SHCT1-9061.8_q2a, illustrating varying pore-pressure conditions during fracture opening. FIA = fluid inclusion assemblage.

bridge are variable (Figure 10B), suggesting significant pore-fluid–pressure fluctuations during fracture opening and cementation.

DISCUSSION

Timing of Fracture Opening and Gas Charge

Our fluid inclusion homogenization temperatures indicate maximum burial temperatures of 180 ± 5°C at the base and 145 ± 5°C at the top of the Mesaverde Group in the southern Piceance Basin. These temperatures are well within the hydrocarbon gas–generation window of 105 to 220°C (Pepper and Corvi, 1995; Pepper and Dodd, 1995) and are consistent with gas generation from coals in the Mesaverde Group (Brown et al., 1986; Johnson and Nuccio, 1986; Cumella and Scheevel, 2008; Yurewicz et al., 2008; Zhang et al., 2008). Our data are also consistent with fluid inclusion homogenization temperatures of 150 to 175°C reported

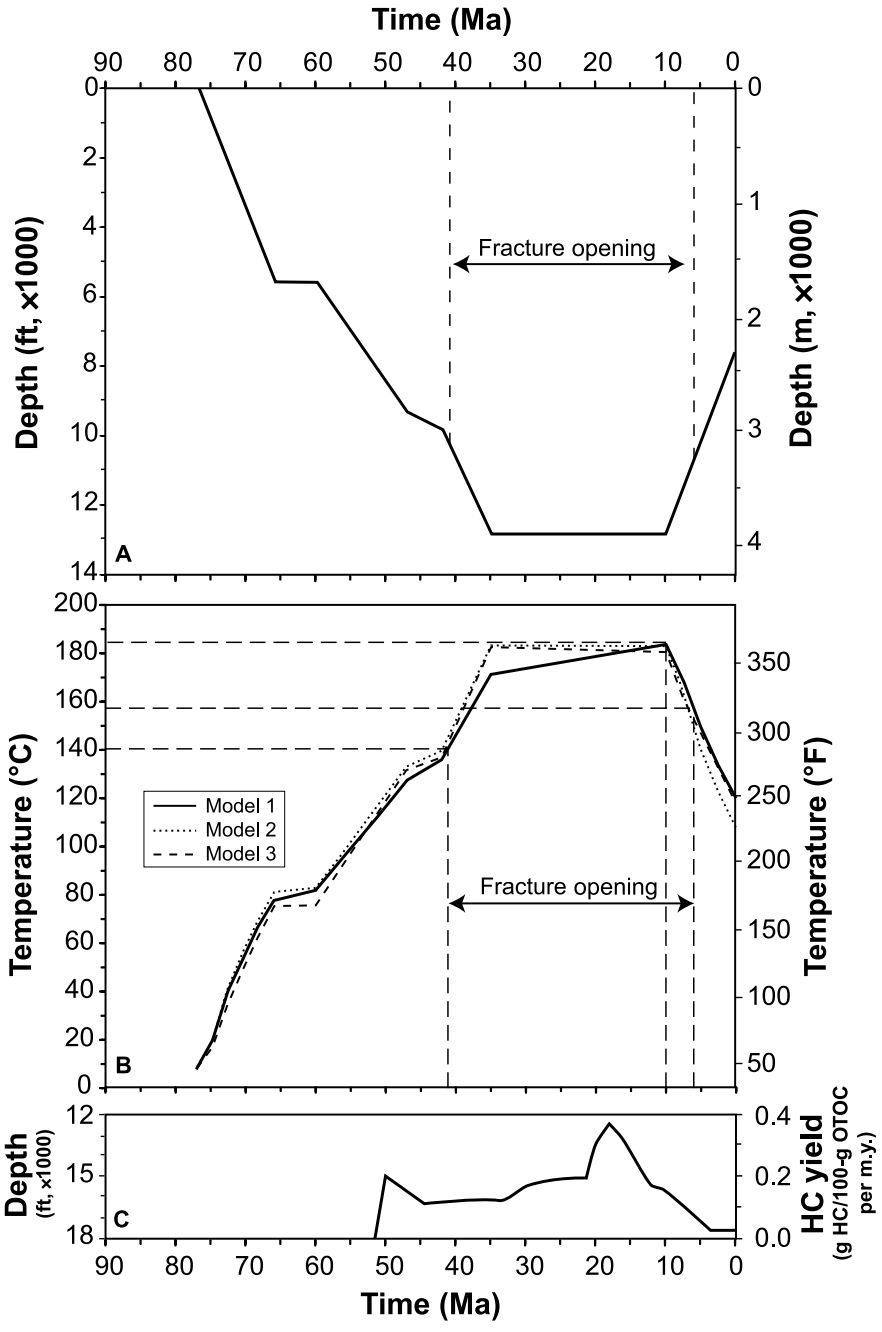

Figure 11. Burial history (A) and thermal evolution model (B) for the base of Mesaverde Group in the southern Piceance Basin (modified from Nuccio and Roberts, 2003). See text for the differences of thermal evolution models 1 to 3. Inferred onset and end of fracture growth relative to temperature model 1 are indicated by long dashed lines. (C) Instantaneous gas yield for the Cameo coals in the MWX1 well showing peak gas generation at approximately 18 Ma in the southern Piceance Basin (modified from Yurewicz et al., 2008). HC = hydrocarbon; OTOC = original total organic carbon.

previously at the MWX site (Barker, 1989; Lorenz and Finley, 1991).

We interpret the observed trends toward higher and, in other samples, cooler fluid inclusion trapping temperatures (Figure 9) to reflect changes in reservoir temperature during increasing burial and later partial exhumation. We did not observe spikes in temperatures within single bridges that would suggest episodic influx of hot water into the reservoir, creating transient anomalies in reservoir temperature (Eichhubl and Boles, 2000). To determine the timing of fracture opening and cementation relative to the burial history and gas charge of the reservoir, we correlated these temperature trends with burial-temperature models obtained using available thermal maturity and pore-fluid–pressure data for the MWX and SHCT wells. Burial- and temperature-history models for the

bottom of the Mesaverde Group were recalculated after Nuccio and Roberts (2003) using the one-dimensional basin-modeling program Genesis 4.8 (ZetaWare, Inc.) and using available vitrinite-reflectance, apatite fission-track, pore-pressure, and wellbore-temperature data (Johnson and Nuccio, 1986; Law et al., 1989; Spencer, 1989b; Kelley and Blackwell, 1990; Yurewicz et al., 2008), as well as our highest fluid inclusion trapping temperatures as an estimate for maximum burial temperatures (Figure 11).

Three models using different boundary conditions were found to match the observations within reasonable limits (Figure 11B). Model 1 uses a uniform transient heat flow at the base of the lithosphere of 80 mW/m^2. This model calculates present-day surface heat-flow values of 101.5 mW/m^2, higher than the 65 to 85 mW/m^2 present-day heat-flow values in the Piceance Basin (Reiter et al., 1975, 1979; Zhang et al., 2008) but comparable to a paleo–heat flow of 77 to 102 mW/m^2 (Kelley and Blackwell, 1990). We attribute this difference to a neglect of a regional igneous heat source during the Oligocene–Pliocene in the southeastern Piceance Basin in our models (Yurewicz et al., 2003; Zhang et al., 2008). We neglected the regional heat source because of constraints of the modeling software. Model 2 assumes a uniform transient heat flow at the base of the sediment column of 90 mW/m^2. Model 3 uses a prescribed uniform thermal gradient of 46°C/km in the sediment column. All of these models assume a mean annual surface temperature of 8°C (Western Regional Climate Center, 2011). This temperature agrees roughly with mean annual surface temperatures in the Rocky Mountain region throughout the Cenozoic (Retallack, 2007). The models obtain maximum burial temperatures at different times: Model 1 attains 185° at approximately 10 Ma, whereas models 2 and 3 attain approximately 183°C at approximately 35 Ma (Figure 11B).

On the basis of the correlation of fluid inclusion temperatures and temperature-history model 1, we conclude that fracture growth in the southern Piceance Basin started at approximately 41 Ma and ended at approximately 6 Ma (Figure 11B). Temperature evolution models 2 and 3 shift the start and end of fracture growth by approximately 1 m.y. without a change in the overall 35-m.y. duration of the time interval. In all models, fracture growth started at approximately 5 Ma before the basin reached maximum burial depth and ended shortly after uplift started. Samples showing minor or no temperature trends over time suggest that some fractures formed over shorter time intervals than the overall duration of fracture opening in the basin.

On the basis of limited fluid inclusion data, Lorenz and Finley (1991) dated the opening of fractures at approximately 40 to 36 Ma, which coincides with a period of Laramide contraction in the basin, corresponding to the fastest burial rates (Lorenz and Finley, 1991). Our onset of fracture formation agrees roughly with their date but extends the duration of fracture opening by approximately 30 m.y. Our data show that fracture development continues after the Laramide contraction is completed and even while the basin is undergoing uplift, supporting a hydrocarbon-generated overpressure mechanism for fracture formation.

Our results on the timing of fracture growth and pressure evolution are consistent with that of the gas-generation models by Yurewicz et al. (2008) for Cameo coals at the MWX1 site (Figure 11C). These models indicate that significant gas generation commenced at approximately 50 Ma, peaked with maximum burial at 18 Ma, and mostly ceased at 6 Ma, concurrent with uplift and exhumation. Similar results were obtained by Zhang et al. (2008) for the northern Piceance Basin. Following Law (2002), with uplift and exhumation, the reservoir entered a stage in which gas loss out of the system dominates over charge that will ultimately result in an underpressured system, such as the San Juan and Denver basins (Law and Dickinson, 1985; Law and Spencer, 2004). Observed present-day elevated pressure gradients in the southern Piceance Basin are thus considered remnants of the stage of dominant gas charge.

Quartz diagenetic modeling by Ozkan (2010) and Ozkan et al. (2011), using realistic quartz-precipitation kinetics (Lander et al., 2008) and calibrated by petrographic point counts and basin models from the Mamm Creek area, demonstrates

that the Williams Fork sandstones reached present-day porosity values between 55 and 25 Ma. These results indicate that the reservoir was tight at the time of gas maturation and charge, a conclusion consistent with those of previous diagenetic studies (Pitman et al., 1989; Dutton et al., 1993). The quartz diagenetic models are also consistent with K-Ar dates of pore-lining illite of 55 to 37 Ma and of pore-filling illite of approximately 50 to 30 Ma by Stroker and Harris (2009).

Pore-Fluid–Pressure Evolution

Present-day pressure gradients in the southern Piceance Basin increase gradually from a hydrostatic gradient of 9.9 MPa/km (0.43 psi/ft) at the top of the Mesaverde gas-saturated interval to approximately 18 MPa/km (0.8 psi/ft) at the base of the Mesaverde Group reaching pore-fluid pressures of approximately 45 MPa (6500 psi) (Spencer, 1987; Nelson, 2003a, b; Cumella and Scheevel, 2008). Our trapping-pressure estimates of fluid inclusion of 55 to 110 MPa (7977–15,954 psi) (Figure 9) indicate that paleo–pore pressures reached near-lithostatic pressures that are approximately twice as high as present-day values close to maximum burial and at the time of incipient fracture growth. Although fluid inclusions do not record the pressure evolution before the inception of fracturing, our results indicate that pore pressures had reached peak levels at the time that fracture growth began and that these high pressures were associated with the presence of a free, methane-rich hydrocarbon phase.

This modern pore-fluid–pressure gradient of approximately 18 MPa/km (1 psi/ft) observed in the gas-saturated zone of the Mesaverde Group, reaching maximum overpressures at the base of the continuous gas zone, is in contrast to the pressure profile expected for a free gas column in a conventional trap where the pressure gradient is controlled by the density of the buoyant gas phase (Spencer, 1987; Swarbrick and Osborne, 1998; Cumella and Scheevel, 2005, 2008; Nelson, 2011). In such conventional reservoirs, overpressure reaches a maximum at the top of the gas column and decreases toward the gas-water interface. The observed pressure gradient is inconsistent with a free buoyant gas column but indicates that gas was either generated within the Mesaverde Group and/or that gas charge predates compaction (Swarbrick and Osborne, 1998). The timing of high pore-fluid pressures at close to peak burial and the occurrence of these high pressures in the presence of a gas phase do not support high pressures caused by compaction disequilibrium. Quartz diagenetic modeling (Ozkan, 2010; Ozkan et al., 2011), pore-lining illite dating (Stroker and Harris, 2009), and our timing of fracture opening show that the Mesaverde sandstones compacted and cemented to present-day low-porosity and low-permeability values well before fracturing and that associated overpressuring occurred. Although we cannot rule out compaction disequilibrium to have contributed to some overpressure generation during prograde burial, the high near-lithostatic pressures in the presence of a gas phase at maximum burial and the continuation of these high pressures during incipient exhumation are consistent with overpressure generation during gas maturation and charge.

The inferred link between near-lithostatic pore-fluid pressures and gas generation and charge is supported by the observed lack of systematic trends in trapping pressure over time. This variability in trapping pressure suggests that pore-fluid–pressure conditions were highly dynamic while the formation was at peak burial and during early exhumation. These dynamic conditions could reflect processes at the scale of a single fracture or at reservoir scale. Dynamically varying pore-fluid–pressure conditions at the fracture scale could result from cyclic fracture growth consistent with the crack-seal mechanism of episodic fracture opening and cementation, in which each fracture-opening increment results in a small drop in local pore-fluid pressure (Beach, 1980). Alternatively, or in addition, reservoir-scale fluctuations in pore-fluid pressure could have resulted from episodic releases of high-pressure methane from deeper sections of the reservoir into shallower sections along fracture and fault conduits. Because rocks are generally weak in tension, with tensile strength in the range

of 1 to 10 MPa (145–1450 psi) (Atkinson and Meredith, 1987), observed variation in pore-fluid pressure greater than 10 to 50 MPa (1450–7252 psi) is likely to reflect reservoir-scale pressure variations that are presumably caused by pulses of upward-migrating high-pressure gas either into or out of the formation using fracture- and fault-flow pathways. Such variability in pore-fluid pressure would not be expected if the pore pressure were the result of compaction disequilibrium during burial but instead suggests an active process of pore-pressure generation at maximum burial conditions. Such a process is consistent with the generation of gas within the Mesaverde Group and possibly from deeper sources, with faults and connected fracture systems serving as charge conduits of highly pressured gas.

Several lines of evidence exist of highly pressured gas sourced from the underlying Mancos Shale. Recent drilling in the Piceance and other Rocky Mountain basins has revealed that an abundant gas resource is present in the Mancos Shale. Pressure gradients encountered in some of these Mancos wells have been greater than 0.01 MPa/m (0.90 psi/ft). Isotopic and gas-composition data indicate that a significant component of the gas produced from Mesaverde may have been sourced from the Mancos Shale (Wilson et al., 1998; Lillis et al., 2008).

Formation of Natural Fractures Intrinsic to Gas Charge

The timing of fracture opening around peak burial conditions, the ubiquitous presence of methane-rich inclusions, and near-lithostatic pore-fluid pressures during fracture opening indicate that fracture growth is intrinsic to gas formation and charge of these reservoirs. The resulting increase in pore-fluid pressure aided the formation of a pervasive natural fracture network, which allowed upward gas migration and charge of intersected sandstone bodies, as well as formation of a continuous gas interval in the Mesaverde Group (Figures 2, 4). Cumella and Scheevel (2008) and Cumella (2010) proposed that sandstones intersected by well-connected fracture and fault systems received a high gas charge and are thus characterized by lower water saturation, whereas sandstone bodies charged through poorly connected fracture systems received a lesser gas charge, with resultant higher water saturation. Observed variations in the ratio of two-phase aqueous inclusions to single-phase hydrocarbon gas inclusions (Table 1) may reflect such differences in primary gas charge. Macro- and microfracture size-spacing data from the SHCT1 well indicate a characteristic spacing of open fractures (mechanical aperture, >0.1 mm) of 0.6 m (2.0 ft) (Hooker et al., 2009). Whereas connectivity of these fractures is difficult to assess on the basis of core data, numerical simulations by Philip et al. (2005) on fractured carbonate reservoirs with a matrix permeability of approximately 1 md suggest that even a poorly connected, widely spaced (10-m [33-ft]) fracture system increases the permeability two- to tenfold as compared with unfractured host rock. The more closely spaced fractures in the Mesaverde sandstones could thus contribute significantly to an increase in permeability during both gas charge and production.

The timing of fracture formation concurrent with gas maturation, the fracture growth under high, near-lithostatic pore-fluid–pressure conditions, and the long duration of fracture growth indicate fracture growth as an inherent component of Piceance Basin tight-gas reservoirs. The universal presence of natural fractures in tight-gas sandstone reservoirs, including those in the Green River Basin, was recognized previously (Dutton et al., 1993; Laubach et al., 2004a), as has the close association of fracture opening with gas maturation and charge (Becker et al., 2010), suggesting that this pattern applies to tight-gas sandstone reservoirs beyond the Piceance Basin. Our view stands in contrast to that of Shanley et al. (2004), who portrayed fractures as incidental to tight-gas sandstone reservoirs. Pore pressures in the model of Shanley et al. (2004) would be limited by hydrocarbon column height and thus would likely remain below the fracture gradient in thin fluvial sandstone lenses of the Mesaverde Group. Fracture opening would be incidental. Gas generation within the reservoir in the basin-centered gas accumulation

model allows for protracted and possibly repeated cycles of pore-fluid–pressure buildup. Buoyancy-generated overpressure by hydrocarbon charge from deeper sources and compaction disequilibrium in the conventional trap model would likely be a singular event. We concur with Shanley et al. (2004) that stratigraphic architecture may affect gas distribution in these reservoirs but note that stratigraphic controls would also affect diagenetic and fracture processes. Under deep burial conditions characteristic of tight-gas reservoirs in which porosity consists mostly of secondary and fracture porosity, primary depositional stratigraphic controls on gas distribution and flow would likely be masked by later diagenetic and fracture processes.

Furthermore, the suggestion by Shanley et al. (2004, 2007) that gas charge and migration occurred well in advance of maximum burial and permeability reduction is unlikely in the case of the Mesaverde sandstone reservoirs in the Piceance Basin (Figure 5). The high pressures indicated by our fluid inclusion data are likely a consequence of a low-permeability system in which gas was generated faster than the rate at which it was lost from the system, and these high pressures would be unlikely in a system with good permeability.

CONCLUSIONS

Fluid inclusions trapped in quartz fracture-filling cement provide a record of fluid composition, temperature, and pressure during natural fracture growth, allowing tests of some of the fundamental aspects of the basin-centered, continuous gas accumulation model as it applies to the southern Piceance Basin. Scanning electron microscopy–catholuminescence imaging reveals textures that demonstrate fracture cement precipitation concurrent with fracture opening and growth. Fluid inclusions trapped during fracture growth are saturated with a methane-rich hydrocarbon fluid, indicating that fracture growth was concurrent with gas generation and charge. Fluid inclusion homogenization temperatures provide trends in trapping temperatures that increase from approximately 140 to 185°C and then decrease again to approximately 158°C. We interpret these trends to reflect fracture growth while the reservoir was passing through maximum burial conditions. On the basis of these microthermometric results and thermal-maturation models, we infer that fracture growth occurred over 35 m.y., ending at approximately 6 Ma, with the onset of uplift and exhumation. Pore-fluid pressures of 55 to 110 MPa (7977–15,954 psi), calculated using Raman spectroscopic analyses and equations of state modeling, indicate fracture opening at near-lithostatic pressures, consistent with natural fracture opening aided by methane generation. Observed variability in pore-fluid pressure over time is interpreted to reflect dynamic conditions of episodic gas charge. Protracted evolution of a pervasive fracture system concurrent with gas maturation and reservoir charge is consistent with basin-centered gas accumulation models that consider natural fractures as an intrinsic component of the reservoir.

REFERENCES CITED

Atkinson, B. K., and P. G. Meredith, 1987, Experimental fracture mechanics data for rocks and minerals, *in* B. K. Atkinson, ed., Fracture mechanics of rock: Academic Press, London, United Kingdom, p. 477–526.

Barker, C. E., 1989, Fluid inclusion evidence for paleotemperatures within the Mesaverde Group, Multiwell Experiment site, Piceance Basin, Colorado, *in* B. E. Law and C. W. Spencer, eds., Geology of tight-gas reservoirs in the Pinedale anticline area, Wyoming, and at the Multiwell Experiment site, Colorado: U.S. Geological Survey Bulletin 1886-B, 11 p.

Beach, A., 1980, Numerical models of hydraulic fracturing and the interpretation of syntectonic veins: Journal of Structural Geology, v. 2, p. 425–438, doi:10.1016/0191-8141(80)90004-8.

Becker, S. P., P. Eichhubl, S. E. Laubach, R. M. Reed, R. H. Lander, and R. J. Bodnar, 2010, A 48-m.y. history of fracture opening, temperature, and fluid pressure: Cretaceous Travis Peak Formation, East Texas Basin: Geological Society of America Bulletin, v. 122, p. 1081–1093, doi:10.1130/B30067.1.

Bodnar, R. J., 1993, Revised equation and table for determining the freezing-point depression of H_2O-NaCl solutions: Geochimica et Cosmochimica Acta, v. 57, p. 683–384, doi:10.1016/0016-7037(93)90378-A.

Bodnar, R. J., 2003, Reequilibration of fluid inclusions, *in* I. Samson, A. Anderson, and D. Marshall, eds., Fluid

inclusions: Analysis and interpretation: Mineralogical Association of Canada Short Course 32, p. 213–231.

Brown, C. A., T. M. Smagala, and G. R. Haefele, 1986, Southern Piceance Basin model: Cozzette, Corcoran and Rollins sandstones, *in* C. W. Spencer and R. F. Mast, eds., Geology of tight gas reservoirs: AAPG Studies in Geology 24, p. 207–219.

Byrnes, A. P., R. M. Cluff, and J. C. Webb, 2009, Analysis of critical permeability, capillary pressures and electrical properties for Mesaverde tight gas sandstones from western U.S. basins: Department of Energy Scientific/Technical Report, Award No. DE-FC26-05NT42660, 355 p.

Camp, W. K., 2008, Basin-centered gas or subtle conventional traps? *in* S. P. Cumella, K. W. Shanley, and W. K. Camp, eds., Understanding, exploring, and developing tight-gas sands: 2005 Vail Hedberg Conference: AAPG Hedberg Series 3, p. 49–61.

Craig, D. P., M. J. Eberhard, M. Ramurthy, C. E. Odegard, and R. Mullen, 2005, Permeability, pore pressure, and leakoff-type distributions in Rocky Mountain basins: Society of Petroleum Engineers Production and Facilities v. 20, p. 48–59.

Cumella, S. P., 2009, Geology of the Piceance Mesaverde gas accumulation, *in* T. Carr, T. D'Agostino, W. Ambrose, J. Pashin, and N. C. Rosen, eds., Unconventional energy resources: Making the unconventional conventional: 29th Annual Gulf Coast Section SEPM Foundation Bob F. Perkins Research Conference, Houston, Texas, December 6–8, 2009, 17 p.

Cumella, S. P., 2010, Important characteristics of Rocky Mountain tight-gas accumulation (abs.): The geology of unconventional gas plays: London, United Kingdom, The Geological Society of London, p. 48–49.

Cumella, S. P., and D. B. Ostby, 2003, Geology of the basin-centered gas accumulation, Piceance Basin, Colorado, *in* K. M. Peterson, T. M. Olson, and D. S. Anderson, eds., Piceance Basin 2003 guidebook: Denver Colorado, Rocky Mountain Association of Geologists, p. 171–193.

Cumella, S. P., and J. Scheevel, 2005, Geology and mechanics of the basin-centered gas accumulation, Piceance Basin, Colorado (abs.): *in* Understanding, exploring and developing tight gas sands: AAPG Hedberg Conference, Vail, Colorado, 5 p.

Cumella, S. P., and J. Scheevel, 2008, The influence of stratigraphy and rock mechanics on Mesaverde gas distribution, Piceance Basin, Colorado, *in* S. P. Cumella, K. W. Shanley, and W. K. Camp, eds., Understanding, exploring, and developing tight-gas sands: 2005 Vail Hedberg Conference, AAPG Hedberg Series 3, p. 137–155.

Duan, Z., and S. Mao, 2006, A thermodynamic model for calculating methane solubility, density and gas phase composition of methane-bearing aqueous fluids from 273 to 523 K and from 1 to 2000 bar: Geochimica et Cosmochimica Acta, v. 70, p. 3369–3386, doi:10.1016/j.gca.2006.03.018.

Dutton, S. P., S. J. Clift, D. S. Hamilton, H. S. Hamlin, T. F. Hentz, W. E. Howard, M. S. Akhter, and S. E. Laubach, 1993, Major low-permeability sandstone gas reservoirs in the continental United States: The University of Texas at Austin, Bureau of Economic Geology Report of Investigations 211, 221 p.

Eichhubl, P., and J. R. Boles, 2000, Rates of fluid flow in fault systems: Evidence for episodic rapid fluid flow in the Miocene Monterey Formation, coastal California: American Journal of Science, v. 300, p. 571–600, doi:10.2475/ajs.300.7.571.

Fall, A., J. D. Rimstidt, and R. J. Bodnar, 2009, The effect of fluid inclusion size on determination of homogenization temperature and density of liquid-rich aqueous inclusions: American Mineralogist, v. 94, p. 1569–1579, doi:10.2138/am.2009.3186.

Goldstein, R. H., and T. J. Reynolds, 1994, Systematics of fluid inclusions in diagenetic minerals: SEPM (Society for Sedimentary Geology) Short Course 31, 199 p.

Hooker, J. N., and S. E. Laubach, 2010, Using empirical trends in fracture size-frequency data to constrain subsurface fracture abundance, *in* Proceedings of the 44th U.S. Rock Mechanics Symposium and 5th U.S.-Canada Rock Mechanics Symposium, Salt Lake City, Utah, June 27–30, 2010: American Rock Mechanics Association 10-325, 11 p.

Hooker, J. N., J. F. W. Gale, L. A. Gomez, S. E. Laubach, R. Marrett, and R. M. Reed, 2009, Aperture-size scaling variations in a low-strain opening-mode fracture set, Cozzette Sandstone, Colorado: Journal of Structural Geology, v. 31, p. 707–718, doi:10.1016/j.jsg.2009.04.001.

Johnson, R. C., 1989, Geologic history and hydrocarbon potential of Late Cretaceous–age, low-permeability reservoirs, Piceance Basin, western Colorado: U.S. Geological Survey Bulletin 1787-E, 51 p.

Johnson, R. C., and V. F. Nuccio, 1986, Structural and thermal history of the Piceance Creek Basin, western Colorado, in relation to hydrocarbon occurrence in the Mesaverde Group, *in* C. W. Spencer and R. F. Mast, eds., Geology of tight gas reservoirs: AAPG Studies in Geology 24, p. 165–205.

Johnson, R. C., and D. D. Rice, 1990, Occurrence and geochemistry of natural gases, Piceance Basin, northwestern Colorado: AAPG Bulletin, v. 74, p. 805–829.

Kelley, S. A., and D. D. Blackwell, 1990, Thermal history of the Multiwell Experiment (MWX) site, Piceance Basin, northwestern Colorado, derived from fission-track analysis: Nuclear Tracks and Radiation Measurements, v. 17, p. 331–337, doi:10.1016/1359-0189(90)90055-3.

Koepsell, R., S. P. Cumella, and D. Uhl, 2003, Applications of borehole images in the Piceance Basin, *in* K. M. Peterson, T. M. Olson, and D. S. Anderson, eds., Piceance Basin guidebook: Denver, Colorado, Rocky Mountain Association of Geologists, p. 233–251.

Lander, R. H., R. E. Larese, and L. M. Bonnell, 2008, Toward more accurate quartz-cement models: The importance of euhedral versus noneuhedral growth rates: AAPG Bulletin, v. 92, p. 1537–1563, doi:10.1306/07160808037.

Laubach, S. E., 1988, Subsurface fractures and their relationship to stress history in East Texas Basin sandstone: Tectonophysics, v. 156, p. 37–49, doi:10.1016/0040-1951(88)90281-8.

Laubach, S. E., 2003, Practical approaches to identifying

sealed and open fractures: AAPG Bulletin, v. 87, p. 561–579, doi:10.1306/11060201106.

Laubach, S. E., R. H. Lander, L. M. Bonnell, J. E. Olson, and R. M. Reed, 2004a, Opening histories of fractures in sandstone: Geological Society (London) Special Publication, v. 231, p. 1–9.

Laubach, S. E., R. M. Reed, J. E. Olson, R. H. Lander, and L. M. Bonnell, 2004b, Coevolution of crack-seal texture and fracture porosity in sedimentary rocks: Cathodoluminescence observations of regional fractures: Journal of Structural Geology, v. 26, p. 967–982, doi:10.1016/j.jsg.2003.08.019.

Law, B. E., 2002, Basin-centered gas systems: AAPG Bulletin, v. 86, p. 1891–1919.

Law, B. E., and W. W. Dickinson, 1985, Conceptual model for origin of abnormally pressured gas accumulations in low-permeability reservoirs: AAPG Bulletin, v. 69, p. 1295–1304.

Law, B. E., and C. W. Spencer, 2004, Basin-centered gas systems and the Jonah field, *in* J. W. Robinson and K. W. Shanley, eds., Jonah field: Case study of a giant tight-gas fluvial reservoir: AAPG Studies in Geology 52, p. 147–158.

Law, B. E., C. W. Spencer, R. R Charpentier, R. A. Crovelli, R. F. Mast, G. L. Dolton, and C. J. Wandrey, 1989, Estimates of gas resources in overpressured low-permeability Cretaceous and Tertiary sandstone reservoirs, Greater Green River Basin, Wyoming, Colorado, and Utah: Wyoming Geological Association 40th Annual Field Conference Guidebook, p. 39–61.

Lewallen, K. T., R. Zhou, G. Chen, X. Wu, and P. Todd, 2008, Seismic characterization of fractured tight-gas reservoirs (abs.): Rocky Mountain Association of Geologists 3-D Seismic Symposium, Denver, Colorado, March 17, 2008.

Lillis, P. G., G. S. Ellis, M. P. Dempsey, and S. P. Cumella, 2008, Origin of gas in the Mamm Creek field, Piceance Basin, Colorado: AAPG Rocky Mountain Section Meeting Abstracts and Program, Denver, Colorado, July 9–11, 2008.

Lin, F., R. J. Bodnar, and S. P. Becker, 2007, Experimental determination of the Raman CH_4 symmetric stretching (ν_1) band position from 1–650 bar and 0.3–22°C: Application to fluid inclusion studies: Geochimica et Cosmochimica Acta, v. 71, p. 3746–3756, doi:10.1016/j.gca.2007.05.016.

Lorenz, J. C., and S. J. Finley, 1991, Regional fractures 2: Fracturing of Mesaverde reservoirs in the Piceance Basin, Colorado: AAPG Bulletin, v. 75, p. 1738–1757.

Lorenz, J. C., and R. Hill, 1994, Subsurface fracture spacing: Comparison of inferences from slant/horizontal and vertical cores: Society of Petroleum Engineers Formation Evaluation 9, p. 66–72.

Lorenz, J. C., D. M. Heinze, J. A. Clark, and C. A. Searls, 1985, Determination of widths of meander-belt sandstone reservoirs from vertical downhole data, Mesaverde Group, Piceance Creek Basin, Colorado: AAPG Bulletin, v. 69, p. 710–721.

Lorenz, J. C., N. R. Warpinski, P. T. Branagan, and A. R. Sattler, 1989, Fracture characteristics and reservoir behavior of stress-sensitive fracture systems in flat-lying lenticular formations: Journal of Petroleum Technology, v. 41, p. 615–622, doi:10.2118/15244-PA.

Nelson, P. H., 2003a, Subsurface pressures from drillstem tests, Uinta and Piceance basins, Utah and Colorado, *in* USGS Uinta-Piceance Assessment Team, Comp., Petroleum systems and geologic assessment of oil and gas in the Uinta-Piceance Province, Utah and Colorado (chapter 14): U.S. Geological Survey Digital Data Series 69-B, 24 p. (CD-ROM).

Nelson, P. H., 2003b, A review of the Multiwell Experiment, Williams Fork and Iles formations, Garfield County, Colorado, *in* USGS Uinta-Piceance Assessment Team, Comp., Petroleum systems and geologic assessment of oil and gas in the Uinta-Piceance Province, Utah and Colorado (chapter 15): U.S. Geological Survey Digital Data Series 69-B, 32 p. (CD-ROM).

Nelson, P. H., 2011, Pore-throat sizes in sandstones, siltstones, and shale: Reply: AAPG Bulletin, v. 95, p. 1448–1453, doi:10.1306/12141010159.

Nuccio, V. F., and L. N. R. Roberts, 2003, Thermal maturity and oil and gas generation history of petroleum systems in the Uinta-Piceance Province, Utah and Colorado, *in* USGS Uinta-Piceance Assessment Team, Comp., Petroleum systems and geologic assessment of oil and gas in the Uinta-Piceance Province, Utah and Colorado (chapter 4): U.S. Geological Survey Digital Data Series 69-B, 39 p. (CD-ROM).

Olson, J. E., S. E. Laubach, and R. H. Lander, 2009, Natural fracture characterization in tight-gas sandstones: Integrating mechanics and diagenesis: AAPG Bulletin, v. 93, p. 1535–1549, doi:10.1306/08110909100.

Ozkan, A., 2010, Structural diagenetic attributes of Williams Fork sandstones with implications for petrophysical interpretation and fracture prediction, Piceance Basin, Colorado: Ph.D. dissertation, University of Texas at Austin, Austin, Texas, 249 p.

Ozkan, A., S. P. Cumella, K. L. Milliken, and S. E. Laubach, 2011, Prediction of lithofacies and reservoir quality using well logs, Late Cretaceous Williams Fork Formation, Piceance Basin, Colorado: AAPG Bulletin, v. 95, p. 1699–1723, doi:10.1306/01191109143.

Patterson, P. E., K. Kronmueller, and T. D. Davies, 2003, Sequence stratigraphy of the Mesaverde Group and Ohio Creek conglomerate, northern Piceance Basin, Colorado, *in* K. M. Peterson, T. M. Olson, and D. S. Anderson, eds., Piceance Basin guidebook: Denver, Colorado, Rocky Mountain Association of Geologists, p. 115–128.

Pepper, A. S., and P. J. Corvi, 1995, Simple kinetic models of petroleum formation. Part 1: Oil and gas generation form kerogen: Marine and Petroleum Geology, v. 12, p. 291–319, doi:10.1016/0264-8172(95)98381-E.

Pepper, A. S., and T. A. Dodd, 1995, Simple kinetic models of petroleum formation. Part 2: Oil-gas cracking: Marine and Petroleum Geology, v. 12, p. 321–340, doi:10.1016/0264-8172(95)98382-F.

Philip, Z. G., J. W. Jennings, J. E. Olson, S. E. Laubach, and J. Holder, 2005, Modeling coupled fracture-matrix fluid flow in geomechanically simulated fracture networks:

Society of Petroleum Engineers Reservoir Evaluation and Engineering, v. 8, p. 300–309.

Pitman, J. K., and E. S. Sprunt, 1987, Origin and distribution of fractures in lower Tertiary and Upper Cretaceous rocks, Piceance Basin, Colorado, and their relation to the occurrence of hydrocarbons, *in* C. W. Spencer and R. L. Mast, eds., Geology of tight gas reservoirs: AAPG Studies in Geology 24, p. 221–233.

Pitman, J. K., C. W. Spencer, and R. M. Pollastro, 1989, Petrography, mineralogy, and reservoir characteristics of the Upper Cretaceous Mesaverde Group in the east-central Piceance Basin, Colorado: U.S. Geological Survey Bulletin 1787-G, 31 p.

Ramsay, J. G., 1980, The crack-seal mechanism of rock deformation: Nature, v. 284, p. 135–139, doi:10.1038/284135a0.

Reiter, M., C. L. Edwards, H. Hartman, and C. Weidman, 1975, Terrestrial heat flow along the Rio Grande rift, New Mexico and southern Colorado: Geological Society of America Bulletin, v. 86, p. 811–818, doi:10.1130/0016-7606(1975)86<811:THFATR>2.0.CO;2.

Reiter, M., A. J. Mansure, and C. Shearer, 1979, Geothermal characteristics of the Colorado Plateau: Tectonophysics, v. 61, p. 183–195, doi:10.1016/0040-1951(79)90297-X.

Retallack, G. J., 2007, Cenozoic paleoclimate on land in North America: Journal of Geology, v. 115, p. 274–294, doi:10.1086/512753.

Roedder, E., 1984, Fluid inclusions, *in* P. H. Ribbe, ed., Reviews in mineralogy: Washington, D.C., Mineralogical Society of America, p. 644.

Schmoker, J. W., 2002, Resource-assessment perspective for unconventional gas systems: AAPG Bulletin, v. 86, p. 1993–1999.

Shanley, K. W., R. M. Cluff, and J. W. Robinson, 2004, Factors controlling prolific gas production from low-permeability sandstone reservoirs: Implications for resource assessment, prospect, and risk analysis: AAPG Bulletin, v. 88, p. 1083–1121, doi:10.1306/03250403051.

Shanley, K. W., R. M. Cluff, and J. W. Robinson, 2007, Prolific gas production from low-permeability sandstone reservoirs. Part 2: Reconciling basin history, fluid saturations, gas shows, and capillary pressure (abs.): AAPG Search and Discovery article 90063. http://www.searchanddiscovery.com/documents/2007/070556_62av_abs/images/ndx_shanley.pdf (accessed October 7, 2011).

Spencer, C. W., 1987, Hydrocarbon generation as a mechanism for overpressuring in Rocky Mountain region: AAPG Bulletin, v. 71, p. 368–388.

Spencer, C. W., 1989a, Review of characteristics of low-permeability gas reservoirs in western United States: AAPG Bulletin, v. 73, p. 613–629.

Spencer, C. W., 1989b, Comparison of overpressures at the Pinedale anticline area, Wyoming, and the Multiwell Experiment site, Colorado, *in* B. E. Law and C. W. Spencer, eds., Geology of tight gas reservoirs in the Pinedale anticline area, Wyoming, and at the Multiwell Experiment site, Colorado: U.S. Geological Survey Bulletin 1886-B, 16 p.

Sterner, S. M., and R. J. Bodnar, 1984, Synthetic fluid inclusions in natural quartz. Part 1: Compositional types synthesized and applications to experimental geochemistry: Geochimica et Cosmochimica Acta, v. 48, p. 2659–2668, doi:10.1016/0016-7037(84)90314-4.

Stroker, T., and N. Harris, 2009, K-Ar dating of authigenic illites: Integrating diagenetic history of the Mesa Verde Group, Piceance Basin, NW Colorado (abs.): AAPG Search and Discovery article 110107. http://www.searchanddiscovery.com/documents/2009/110107stroker/ndx_stroker.pdf (accessed October 7, 2011).

Surdam, R. C., 1997, A new paradigm for gas exploration in anomalously pressured tight gas sands in the Rocky Mountain Laramide basins, *in* R. C. Surdam, ed., Seals, traps, and the petroleum system: AAPG Memoir 67, p. 283–298.

Swarbrick, R. E., and M. J. Osborne, 1998, Mechanisms that generate abnormal pressures: An overview, *in* B. E. Law, G. F. Ulmishek, and V. I. Slavin, eds., Abnormal pressure in hydrocarbon environments: AAPG Memoir 70, p. 13–34.

Verbeek, E. R., and M. A. Grout, 1984a, Fracture studies in Cretaceous and Paleocene strata in and around the Piceance Basin, Colorado: Preliminary results and their bearing on a fracture-controlled natural-gas reservoir at the MWX site: U.S. Geological Survey Open File Report 84-156, 30 p.

Verbeek, E. R., and M. A. Grout, 1984b, Prediction of subsurface fracture patterns from surface studies of joints: An example from the Piceance Creek Basin, Colorado, *in* U.S. Geological Survey Open File Report 84-757, p. 75–86.

Western Regional Climate Center, 2011, General climate summary for Rifle, Colorado: Reno, Nevada, Desert Research Institute: http://www.wrcc.dri.edu/cgi-bin/cliMAIN.pl?co7031 (accessed October 4, 2011).

Wilson, M. S., B. G. Gunneson, K. Petersen, R. Honore, and M. M. Laughland, 1998, Abnormal pressures encountered in a deep wildcat well, southern Piceance Basin, Colorado, *in* B. E. Law, G. F. Ulmishek, and V. I. Slavin, eds., Abnormal pressure in hydrocarbon environments: AAPG Memoir 70, p. 195–214.

Yurewicz, D. A., K. M. Bohacs, J. D. Yeakel, and K. Kronmueller, 2003, Source rock analysis and hydrocarbon generation, Mesaverde Group and Mancos Shale, northern Piceance Basin, Colorado, *in* K. M. Peterson, T. M. Olson, and D. S. Anderson, eds., Piceance Basin guidebook: Denver, Colorado, Rocky Mountain Association of Geologists, p. 130–153.

Yurewicz, D. A., K. M. Bohacs, R. E. Kendall, K. Kronmueller, M. E. Maurer, T. C. Ryan, and J. D. Yeakel, 2008, Controls on gas and water distribution, Mesaverde Basin–centered gas play, Piceance Basin, Colorado, *in* S. P. Cumella, K. W. Shanley, and W. K. Camp, eds., Understanding, exploring, and developing tight-gas sands: 2005 Vail Hedberg Conference: AAPG Hedberg Series 3, p. 105–136.

Zhang, E., R. J. Hill, B. J. Katz, and Y. Tang, 2008, Modeling of gas generation from the Cameo coal zone in the Piceance Basin, Colorado: AAPG Bulletin, v. 92, p. 1077–1106, doi:10.1306/04020806015.